Available online at www.sciencedirect.com
SCIENCE DIRECT
Catalysis Today 105 (2005) 244–253
CATALYSIS TODAY
www.elsevier.com/locate/cattod

Subsurface oxygen formation on Pt(1 0 0): Experiments and modeling

Noah McMillan [a], Tanmay Lele [c,1], Christopher Snively [a,b], Jochen Lauterbach [a,*]

[a] Department of Chemical Engineering, University of Delaware, Newark, DE 19716, USA
[b] Department of Materials Science and Engineering, University of Delaware, Newark, DE 19716, USA
[c] School of Chemical Engineering, Purdue University, West Lafayette, IN 47907, USA

Available online 13 June 2005

Abstract

Spatially resolved techniques, such as photoemission electron microscopy (PEEM) and ellipsomicroscopy for surface imaging (EMSI), have been particularly useful in the investigation of pattern formation during CO oxidation on platinum catalysts. One surprising result of these studies has been the discovery of subsurface oxygen on Pt(1 0 0). The formation of subsurface oxygen has been reported previously on Pt(1 0 0) during CO oxidation at low pressures ($<1 \times 10^{-4}$ Torr). This communication reports the formation of subsurface oxygen at intermediate pressures (~0.1 Torr). These observations show that subsurface oxygen plays a role in catalytic CO oxidation and pattern formation, which has implications for catalysts operated at higher pressures. New microkinetic models of CO oxidation that incorporate subsurface oxygen are discussed. Results of these models are qualitatively similar to experimental observations of subsurface oxygen, confirming the importance of this species in the reaction dynamics.

Keywords: Subsurface oxygen; Pattern formation; Pt(100); PEEM; EMSI; CO oxidation

1. Introduction

CO oxidation over noble metal catalysts is one of the most widely studied surface reactions. This system has been found to exhibit complex nonlinear behavior, including reaction rate oscillations and spatiotemporal pattern formation over a wide range of conditions from high vacuum to atmospheric pressures [1,2]. The Langmuir–Hinshelwood model alone cannot explain these phenomena, and detailed experimental investigations are required for the development of more appropriate models.

The surface reconstruction model is a generally accepted explanation for the complex behavior of CO oxidation on Pt(1 0 0) at low pressures ($<1 \times 10^{-4}$ Torr) [3]. The clean Pt(1 0 0) surface spontaneously rearranges from its bulk-like (1×1) termination into a quasi-hexagonal (hex) reconstructed surface. This reconstruction is favored because it minimizes the surface energy in the absence of adsorbates. Lifting of the reconstruction (i.e. recovery of the 1×1 surface) is induced by adsorption of a critical coverage of CO or O_2. The adsorption probability of O_2 on the 1×1 surface is ~0.1, compared to $\sim 10^{-4}$ on the hex surface, therefore the rate of O_2 adsorption increases with the lifting of the hex reconstruction [4–6]. The increasing rate of O_2 adsorption leads to a higher reaction rate with CO to form CO_2, which immediately desorbs at typical reaction temperatures. As a result, the surface coverage decreases and the surface reverts to the hex reconstruction. Repetition of this cycle accounts for reaction rate oscillations and the appearance of spatiotemporal patterns.

One limitation of the surface reconstruction model is that, as in the Langmuir–Hinshelwood model, adsorbates are restricted to the catalyst surface. However, it has been known for some time that adsorbates can penetrate the surface under reaction conditions, in some cases causing significant changes in reaction dynamics and catalytic activity. Such oxygen species have been referred to in the literature as ''bulk oxygen,'' ''dissolved oxygen,'' or ''surface oxide.'' For example, Turner et al. reported a surface oxide on platinum wire that formed during CO oxidation between 100 and 800 Torr and temperatures as low as 520 K [7].

* Corresponding author. Tel.: +1 302 831 6327; fax: +1 302 831 1048.
E-mail address: lauterba@che.udel.edu (J. Lauterbach).
[1] Present address: Departments of Pathology and Surgery, Children's Hospital and Harvard Medical School, Boston, MA 02138, USA.

0920-5861/$ – see front matter © 2005 Elsevier B.V. All rights reserved.
doi:10.1016/j.cattod.2005.02.042

This species was found to be significantly less reactive than chemisorbed oxygen and was thought to be responsible for the observed reaction rate oscillations. Other researchers reported the formation of a less reactive oxygen species only at temperatures above 800 K [8,9]. Ladas et al. proposed that reaction rate oscillations during CO oxidation on Pd(1 1 0) were the result of a periodic storage and removal of oxygen underneath the surface [10]. In this case, the bulk palladium acts as a reservoir for oxygen during the catalytic reaction. Other researchers have reported a dissolved oxygen species on platinum that is distinguished by its low reactivity compared to chemisorbed oxygen. This low reactive species has been used to achieve highly selective partial oxidation, as in the methane to syngas reaction [11–13].

While there is no generally accepted terminology to distinguish these various oxygen species, this paper follows the nomenclature introduced by Dicke et al., who identified three forms of oxygen on Pt(1 0 0) [14]. The authors differentiated between chemisorbed oxygen, subsurface oxygen, and surface oxide mainly by comparison of temperature programmed desorption (TPD) spectra. Chemisorbed oxygen, the most reactive species, desorbs between 600 and 730 K. Subsurface oxygen is less reactive and desorbs between 650 and 770 K. Surface oxide is unreactive and remains stable at temperatures below 1000 K. Subsurface oxygen and chemisorbed oxygen can be reactively removed by exposure to CO or H_2, however surface oxide is chemically inert and can only be removed by thermal decomposition by heating to temperatures above 1000 K.

2. Experimental results and discussion

Imaging techniques such as PEEM and EMSI allow the direct observation of the formation and removal of the oxygen species described above. In fact, imaging of CO oxidation by PEEM was essential to the identification of subsurface oxygen as a unique chemical species. This section reviews low pressure experiments showing the formation and reaction of subsurface oxygen and presents some new observations of subsurface oxygen at higher pressures. The PEEM and EMSI techniques have been described in detail previously [15–19].

2.1. Experiments at low pressure

With the advent of PEEM, it became possible to image a relatively large area (~500 μm diameter) of a working catalyst surface in real time. Areas of different adsorbate coverage are easily distinguished in the images because the contrast of PEEM results from work function differences on the surface. In general, areas of low work function appear bright, whereas areas of high work function appear dark. Hence, in studies of CO oxidation on platinum, CO-covered regions appear bright while O-covered regions appear dark.

Subsurface oxygen was first observed in PEEM images of pattern formation during CO oxidation on Pt(1 1 0) [20]. Very bright areas – much brighter than the clean surface – were observed to form under reaction conditions. Once formed, these areas persisted relatively unchanged for long periods of time (i.e. minutes to hours) and were tentatively ascribed to subsurface oxygen. Similar low work function areas were subsequently reported on Pt(1 0 0) [21]. In these experiments, islands of subsurface oxygen were carefully prepared under controlled conditions. Fig. 1 shows an example of this process. First, the surface is saturated with CO at 360 K. The supply of CO is turned off and O_2 is slowly leaked into the vacuum chamber. After some time, oxygen islands begin to nucleate and grow, typically at a defect on the surface. When the oxygen islands reach the desired size (several 100 μm in diameter), the oxygen supply is turned off. Upon heating the sample to 450 K at a rate of about 3 K/s, a bright fringe of subsurface oxygen is observed around the oxygen island. This fringe grows toward the interior of the island until the entire island was converted to subsurface oxygen. Upon further heating, the brightness continues to increase until the temperature reaches 560–600 K. Heating above 600 K causes the bright area to dim and eventually disappear due to the desorption of subsurface oxygen. The activation energy for the formation of subsurface oxygen was determined to be 60 ± 20 kJ/mol, significantly lower than the activation energy of oxygen desorption (160 kJ/mol) [22].

It is reasonable to assume that low work function areas are due to the presence of subsurface oxygen. When oxygen adsorbs onto platinum, the dipole along the oxygen–platinum bond is directed toward oxygen and away from the surface. The relatively high electron density near oxygen acts as a potential barrier that electrons must overcome in order to be emitted from the surface. If oxygen lies beneath the surface, however, the dipole is directed into the bulk (toward oxygen). In this case, the higher electron density repels electrons bound to the surface, resulting in a lower work function than even the clean surface. Indeed, the work function of subsurface oxygen on Pt(1 0 0) was reported to be up to 1.2 eV lower than that of a clean surface and ~1.7 eV lower than that of chemisorbed oxygen [21]. Auger electron spectroscopy (AES) of these areas confirmed that they contained oxygen, and the observed peak was shifted 1–1.5 eV to lower kinetic energies, as compared to chemisorbed oxygen [21]. ‘‘Impurity oxides’’ due to small amounts of Si and Ca have been reported on platinum, but neither Si nor Ca was detected by AES [21]. Therefore, the formation of subsurface oxygen is only due to the interaction of chemisorbed CO and O with the catalyst surface, and cannot be attributed to the presence of impurities.

Although the formation of subsurface oxygen is attributed to fundamental surface processes, the nonuniformity of this process, proceeding from the edge of a chemisorbed oxygen island toward the interior, suggests that

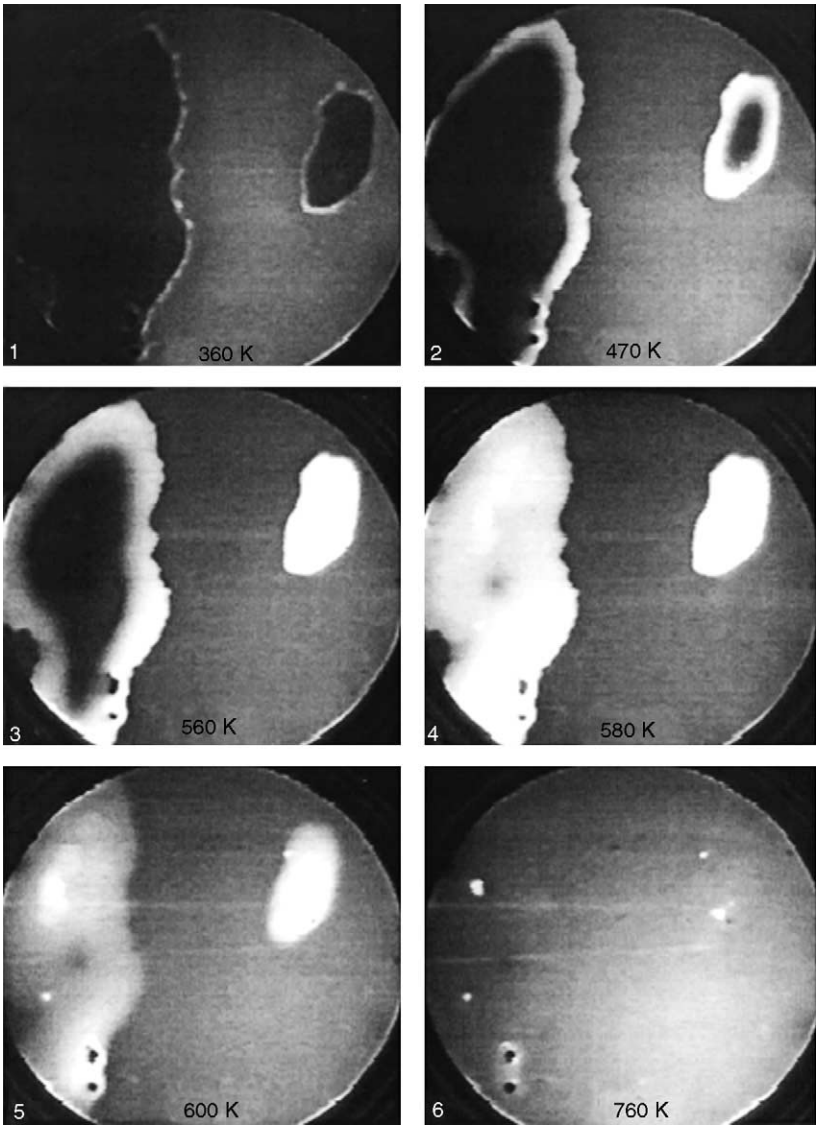

Fig. 1. Images of subsurface oxygen formation from chemisorbed oxygen on Pt(1 0 0). Image diameter = 620 μm. Image reprinted from [21].

it is accompanied by the propagation of some surface structure. Small-spot LEED measurements showed that the surface structure accompanying subsurface oxygen islands is predominantly hex, however, the surface structure below chemisorbed CO- or O-saturated surfaces is 1×1 [23]. Furthermore, the activation energy of the surface phase transition is ~100 kJ/mol, similar to the activation energy of subsurface oxygen formation [23]. This evidence suggests that subsurface oxygen formation is accompanied by a surface transition from 1×1 to hex.

Incorporating these ideas, a mechanism was proposed for the formation of subsurface oxygen on Pt(1 0 0) involving only simple surface processes [23]. A schematic of this mechanism is shown in Fig. 2. Adsorption of CO onto the clean surface lifts the hex reconstruction. When oxygen is dosed into the chamber, chemisorbed oxygen islands begin to grow on the 1×1 surface. When the oxygen is turned off, the CO- and O-covered areas of the surface remain in the 1×1 phase, however the interface between the oxygen islands and the CO-covered surface has a low coverage due to reaction. This clean fringe then reconstructs to the hex phase. The interface between the clean hex surface and the O-covered 1×1 surface allows chemisorbed oxygen to

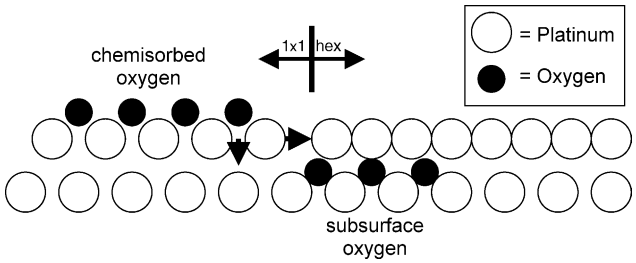

Fig. 2. A proposed mechanism showing the formation of subsurface oxygen at the interface between the O-covered 1×1 surface and the clean hex surface. The formation of subsurface island results in a hex surface with subsurface oxygen lying underneath.

diffuse underneath the surface layer of Pt atoms. As this process proceeds, a subsurface oxygen front propagates across the surface, accompanied by the surface phase transition from the 1×1 phase to the hex phase. This process occurs independently of any reaction between O and CO.

Although subsurface oxygen can be formed from chemisorbed oxygen, it is interesting that the reverse transformation is never observed. In fact, subsurface oxygen can persist relatively unchanged for long times (minutes to hours), even during reaction conditions. The reaction of subsurface oxygen with H_2 and CO was also observed by PEEM [23]. In each case, the subsurface oxygen was reactively removed, but the reaction with subsurface oxygen was slower than the same reaction with chemisorbed oxygen. Similar to the formation of subsurface oxygen, the reactive removal of subsurface oxygen occurs from the edges of the island moving to the interior, again indicating the importance of the surface structure.

2.2. Subsurface oxygen at intermediate pressures

Because it is an electron-based technique, PEEM is limited to the study of reactions at low pressures ($<1 \times 10^{-4}$ Torr), but catalysis in practice occurs at much higher pressures. The development of ellipsomicroscopy for surface imaging has allowed the imaging of pattern formation at pressures higher than possible with PEEM [16]. This section presents new results that demonstrate the importance of subsurface oxygen at intermediate pressures.

Pattern formation at intermediate temperatures and pressures (total pressure of 6×10^{-2} Torr, and a temperature range of 480–615 K) was observed using imaging ellipsometry, however to the best of our knowledge this is the first

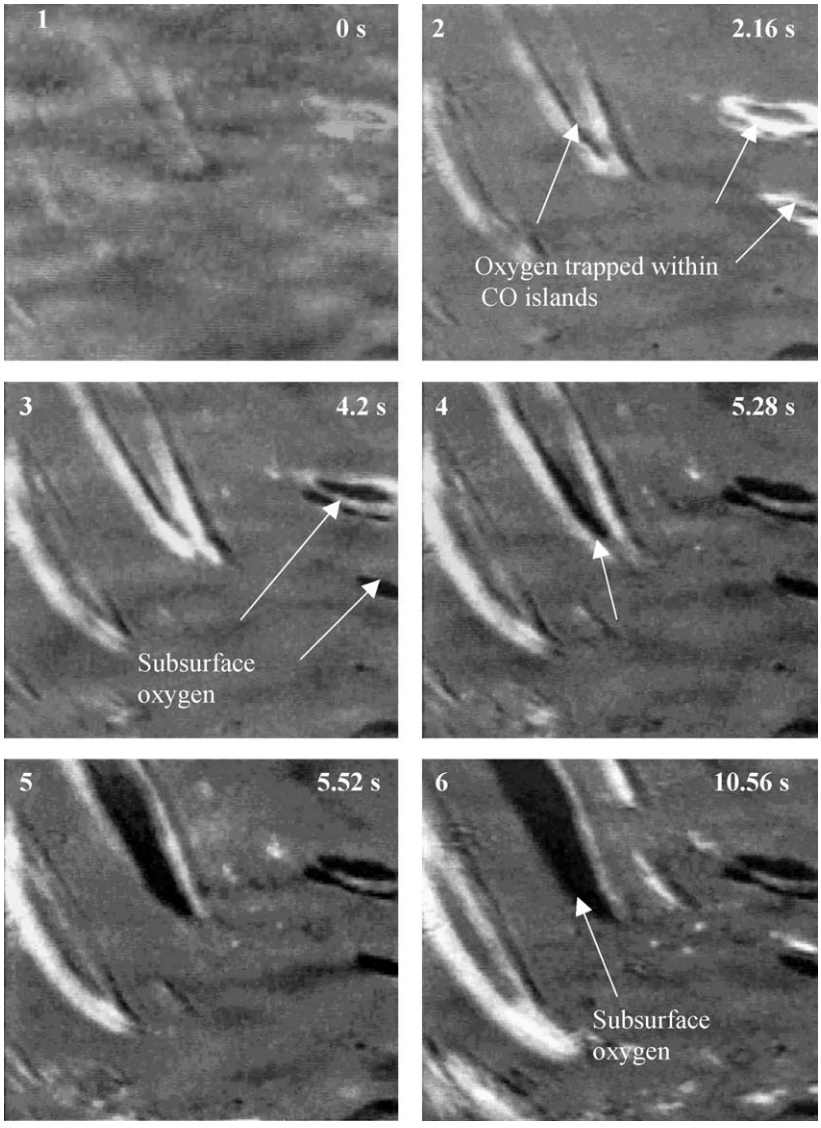

Fig. 3. The conversion of chemisorbed oxygen to subsurface oxygen; image size $\sim$ 1 mm $\times$ 1.25 mm, CO partial pressure = 7.8×10^{-3} Torr, oxygen partial pressure = 5.2×10^{-2} Torr, temperature = 523 K.

report of subsurface oxygen formation under these conditions [24]. EMSI images captured at intermediate pressures during CO oxidation show regions of the Pt(1 0 0) surface with three distinct grayscales. This difference is not a consequence of the work function difference, as in PEEM, but due to differences in optical properties between areas of the surface with different adsorbates. The brightest and intermediate of these grayscales denote chemisorbed CO and O, respectively. Based on comparison to subsurface oxygen on the Pt(1 0 0) surface observed at lower pressures using PEEM, we propose that the darkest areas in EMSI indicate subsurface oxygen.

Fig. 3 shows the formation of subsurface oxygen during pattern formation at a temperature of 523 K, with a CO/O_2 ratio of 0.13, and a total pressure of 6×10^{-2} Torr. Initially, small CO islands nucleate on an O-covered surface. The CO islands grow by surrounding a chemisorbed oxygen island. Three of these surrounded oxygen islands are indicated with arrows in frame 2 of Fig. 3. The islands can be identified as chemisorbed oxygen because they have the same brightness level as the rest of the O-covered surface. By frame 3, two of the chemisorbed oxygen islands have converted to subsurface oxygen, as indicated by the appearance of areas distinctly darker than chemisorbed oxygen. The conversion of chemisorbed oxygen to subsurface oxygen is accompanied by the disappearance of the surrounding CO islands. The same process is shown in the subsequent frames. In frames 4 and 5, the conversion of chemisorbed oxygen to subsurface oxygen starts from the interface between chemisorbed CO and O (indicated by the arrow in frame 4) and proceeds toward the interior of the island as a wave. By frame 6, the entire chemisorbed oxygen island has converted to subsurface oxygen. This is again accompanied by the disappearance of the surrounding chemisorbed CO.

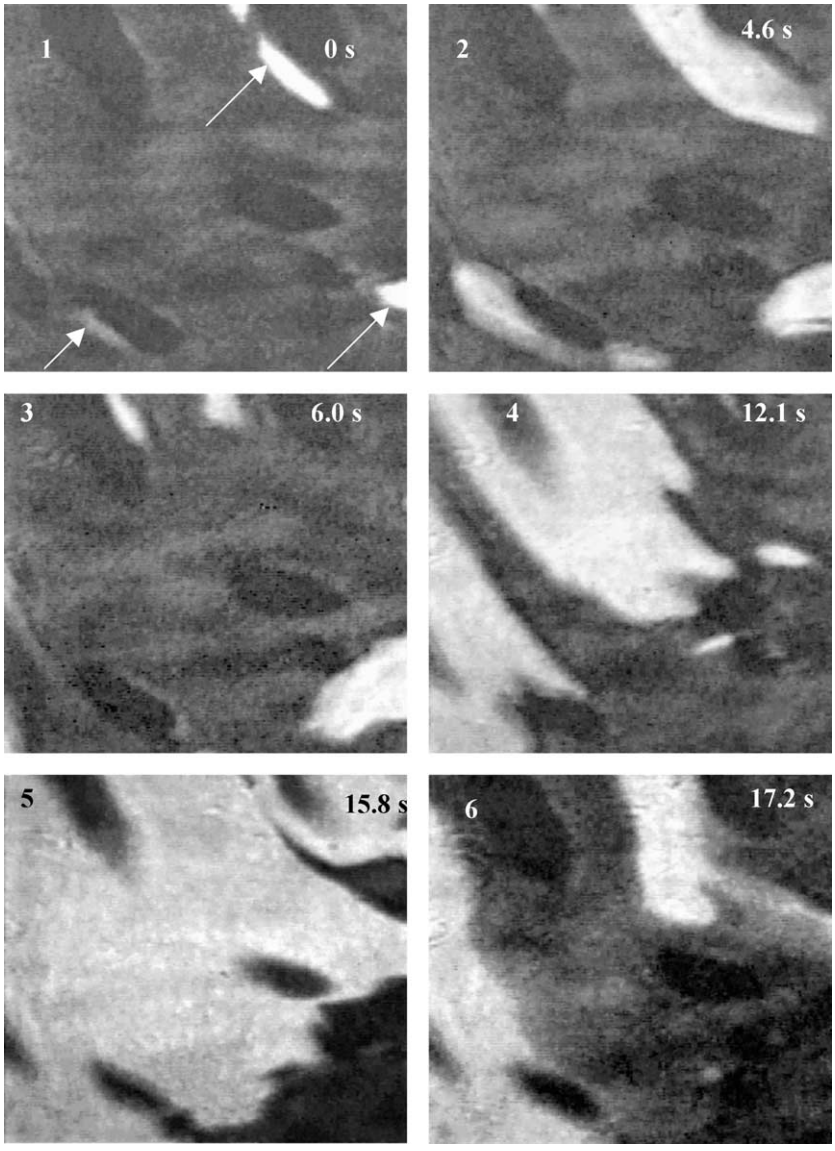

Fig. 4. The role of subsurface oxygen in nucleating CO islands; image size ~ 1 mm × 1.25 mm, CO partial pressure = 0.0138 Torr, oxygen partial pressure = 0.0462 Torr, temperature = 540 K.

This process is identical to observations of subsurface oxygen at low pressure, except that it occurs at a faster rate. The entire process in Fig. 3 (frames 1–6) takes around 11 s compared to the formation of a similarly sized subsurface oxygen island at low pressures ($<10^{-4}$ Torr) which can take more than 1 min.

After formation, subsurface oxygen islands can persist under reaction conditions at intermediate pressures and higher temperatures. Fig. 4 shows the behavior of subsurface oxygen under reaction conditions at 540 K and a feed composition of $CO/O_2 = 0.30$. In frame 1, chemisorbed oxygen covers most of the surface, but several subsurface oxygen islands can still be clearly seen in the image. Three CO islands have nucleated adjacent to a subsurface oxygen area as indicated by arrows. The fact that subsurface oxygen areas are nucleation sites for CO demonstrates that subsurface oxygen does actively participate in pattern formation. The CO islands grow by propagation across the O-covered surface as well as the subsurface oxygen areas. In frame 5, CO covers most of the surface, but by frame 6, the chemisorbed CO has already largely been removed by a propagating wave of chemisorbed oxygen. Even in this final frame, several subsurface oxygen islands are visible on a largely oxygen-covered surface. These islands are roughly the same size, shape, and position as the subsurface oxygen areas in frame 1, demonstrating the stability of subsurface oxygen under reaction conditions. The islands were observed to persist, relatively unchanged, for several minutes of reaction. The same qualitative behavior is also observed at higher temperatures (560 K), where the subsurface oxygen islands are smaller in size and larger in number, so that significant amounts of the surface have subsurface oxygen present. The size of the subsurface oxygen areas is on the order of 10 μm, compared to the ∼100 μm islands observed at 540 K.

3. Modeling

CO oxidation has been the focus of numerous modeling studies addressing a wide range of pressures (from high vacuum to above atmospheric pressure) and materials (from single crystals to supported catalysts). A common approach is to assume Langmuir–Hinshelwood kinetics with dissociative O_2 adsorption [3]. In more sophisticated models, an adsorbate-induced surface phase transition is also considered [25].

As examples of this latter approach, two recent microkinetic models successfully simulate reaction rate oscillations during CO oxidation on Pt(1 0 0) [26,27]. A shortcoming of these models is that they do not address subsurface oxygen. Based on the experimental evidence presented above, subsurface oxygen is present during CO oxidation, and this species should be included in realistic models. This section describes an attempt to incorporate subsurface oxygen into microkinetic models of CO oxidation.

3.1. Microkinetic models

A microkinetic partial differential equation (PDE) approach has been used successfully to simulate reaction rate oscillations and pattern formation with subsurface oxygen on Pt(1 1 0) [28–30]. In this case, the formation and removal of subsurface oxygen was shown to be necessary for the formation of certain types of spatiotemporal patterns, such as standing waves.

A similar PDE approach can also be used to model CO oxidation on Pt(1 0 0). We propose a simple model of the controlled formation of subsurface oxygen from chemisorbed oxygen, a process that has previously been observed experimentally [23]. In the experiments, an oxygen island is prepared on a CO-covered surface. When the island is heated to 450 K, the chemisorbed oxygen begins to convert to subsurface oxygen, first at the fringe and then propagating toward the interior. This process is similar to that shown in Fig. 1.

In order to model the conversion of chemisorbed oxygen to subsurface oxygen, three elemental processes are considered:

$O^{1\times1} \xrightarrow{k_1} O^{hex}_{sub}$

(migration of chemisorbed oxygen to the subsurface)

$hex \xrightarrow{k_2} 1\times1$ (phase transition of hex to 1×1 (favored by chemisorbed oxygen))

$1\times1 \xrightarrow{k_3} hex$ (phase transition of 1×1 to hex (favored by subsurface oxygen))

In mathematical terms, this leads to a model with three PDEs:

$$\frac{\partial\theta_O^{1\times1}}{\partial t} = -k_1\theta_O^{1\times1}(1-\theta^{1\times1})(0.6-\theta^{hex}_{O_{sub}}) + D_O^{1\times1}\frac{\partial^2\theta_O^{1\times1}}{\partial x^2} \quad (1)$$

$$\frac{\partial\theta^{hex}_{O_{sub}}}{\partial t} = k_1\theta_O^{1\times1}(1-\theta^{1\times1})(0.6-\theta^{hex}_{O_{sub}}) \quad (2)$$

$$\frac{\partial\theta^{1\times1}}{\partial t} = k_2\theta_O^{1\times1}(1-\theta^{1\times1}) - k_3\theta^{hex}_{O_{sub}}\theta^{1\times1} \quad (3)$$

These three equations account for changes in the coverage of oxygen adsorbed on the 1×1 surface, $\theta_O^{1\times1}$, the coverage of subsurface oxygen on the subsurface, $\theta^{hex}_{O_{sub}}$, and the fraction of the surface in the 1×1 phase, $\theta^{1\times1}$. In Eq. (1), the chemisorbed oxygen balance equation, the first term is the rate at which oxygen migrates to the subsurface. In addition to the Arrhenius rate constant, k_1, the term includes three more parts. First, the rate is proportional to the coverage of O on the 1×1 surface that is available to migrate.

Second, the rate is proportional to the fraction of the surface in the hex phase ($1 - \theta^{1\times1}$). This accounts for the experimental observation that subsurface oxygen only forms at the interface between hex and 1×1 sufaces. (In other words, this prevents subsurface oxygen from initially forming in the interior of a chemisorbed oxygen island. Finally, the rate is proportional to the number of available subsurface sites ($0.6 - \theta^{\text{hex}}_{\text{O}_{\text{sub}}}$). This formulation assumes that there are as many possible subsurface ''sites'' for subsurface oxygen as there are surface sites for chemisorbed oxygen. (0.6 ML corresponds to a saturated chemisorbed oxygen surface.) Formation of subsurface oxygen blocks some of the subsurface sites and results in a reduced rate of subsurface oxygen formation, so that there is a limit to subsurface oxygen formation at which the subsurface is saturated. The second term in the chemisorbed oxygen balance describes the diffusion of oxygen across the surface. Although surface diffusion for oxygen is quite slow at these temperatures, it was found to be important in simulations.

Eq. (2), the balance equation for subsurface oxygen, contains only a single term for the formation of subsurface oxygen. This term is identical (but opposite in sign) to the first term in the chemisorbed oxygen balance.

Eq. (3) accounts for the surface phase transition and consists of two terms. The first term indicates that growth of the 1×1 surface is favored by adsorption of oxygen. This is consistent with experimental studies which have shown that the hex reconstruction is lifted by adsorption of a critical coverage of O (or CO). The second term indicates that the fraction of the 1×1 surface decreases when the subsurface coverage increases. This follows from the experimental fact that subsurface oxygen has only been observed under the hex phase. The presence of subsurface oxygen therefore stabilizes the hex surface even in the presence of chemisorbed CO. This equation does not address the adsorbate-induced surface phase transition that has been included in previous models, but only the surface phase transition that occurs as a result of subsurface oxygen formation. According to our model, the reconstruction to the hex phase is driven by the formation of subsurface oxygen and not by the traditional adsorbate model. Although the surrounding adsorbate-free surface will reconstruct to the hex phase in the typical manner, the coverage of chemisorbed oxygen within the island is sufficient to stabilize the 1×1 surface, absent the subsurface species.

Table 1 lists the parameters used in the simulation. The problem is solved in one dimension with no-flux boundary

Table 1
List of values used in PDE model for formation of subsurface oxygen

Parameter	Value		Reference
	Pre-exponential	Activation energy (kJ/mol)	
k_1	$3 \times 10^6\ \text{s}^{-1}$	62.76	[23,28]
k_2	$1 \times 10^{-1}\ \text{s}^{-1}$	0	–
k_3	$1 \times 10^{-1}\ \text{s}^{-1}$	0	–
$D_{\text{O}}^{1\times1}$	$2.4 \times 10^{-3}\ \text{cm}^2\ \text{s}^{-1}$	126	[28]

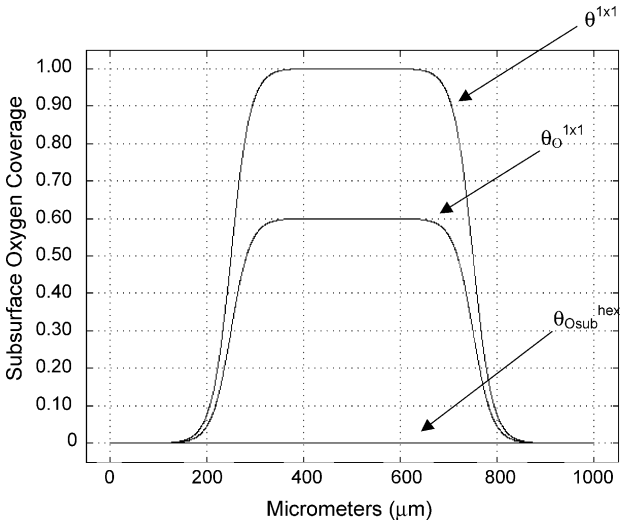

Fig. 5. Initial conditions for simulation of subsurface oxygen formation.

conditions. The initial conditions are shown in Fig. 5. Initially, a chemisorbed oxygen island lies on top of a 1×1 surface. Because of the method used experimentally to prepare chemisorbed oxygen islands, the immediately surrounding surface is adsorbate-free and in the hex phase. The results of this simulation at 450 K agree qualitatively with the experimental results. Fig. 6 shows that the transformation of the oxygen from the chemisorbed state to the subsurface state occurs in a wave-like manner, beginning at the edges of the island and proceeding toward the interior. The subsurface oxygen wave moves at a speed of approximately 1.1 μm/s. This result is consistent with the wave speed of 1 μm/s that was experimentally observed at 450 K [23].

A similar model can be written to simulate the reactive removal of subsurface oxygen by CO, also observed by Lauterbach et al. [23]. In the experiment, CO was adsorbed onto a previously prepared island of subsurface oxygen. With the adsorption of CO, the entire image darkened

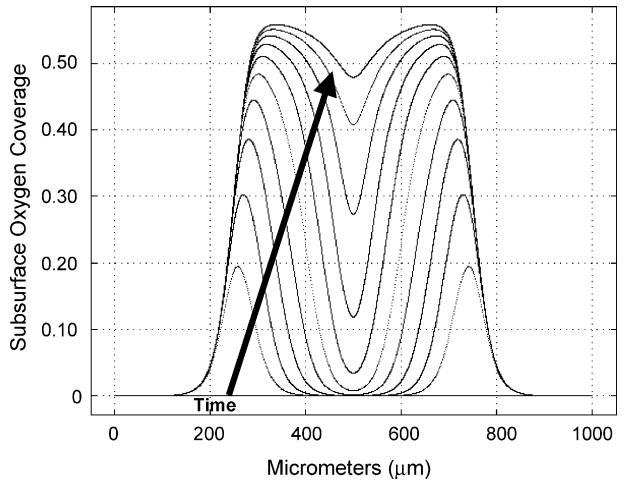

Fig. 6. Simulation results for subsurface oxygen formation at 450 K from 0 to 300 s. Time between profiles is 30 s.

slightly, and the subsurface oxygen island remained noticeably brighter than the areas covered by only CO.

The processes considered in this model are

$$CO(g) + *^{1\times1} \overset{k_1,k_{-1}}{\longleftrightarrow} CO^{1\times1}$$

(adsorption/desorption of CO on 1 × 1 sites)

$$CO(g) + *^{hex} \overset{k_2,k_{-2}}{\longleftrightarrow} CO^{hex}$$

(adsorption/desorption of CO on hex sites)

$$CO^{1\times1} + O^{hex}_{sub} \xrightarrow{k_3} CO_2$$

(subsurface oxygen reaction at edge)

$$CO^{hex} + O^{hex}_{sub} \xrightarrow{k_4} CO_2$$

(subsurface oxygen reaction in interior)

$$CO^{1\times1} + *^{hex} \overset{k_5,k_{-5}}{\longleftrightarrow} CO^{hex} + *^{1\times1}$$

(migration of CO between hex and 1 × 1 sites)

$$hex \xrightarrow{k_6} 1\times1 \quad \text{(phase transition of hex to 1 × 1)}$$

$$1\times1 \xrightarrow{k_7} hex \quad \text{(phase transition of 1 × 1 to hex)}$$

The model equations are as follows:

$$\frac{d\theta^{1\times1}_{CO}}{dt} = k_1 p_{CO} s^{1\times1}_{CO}(\theta^{1\times1} - \theta^{1\times1}_{CO}) - k_{-1}\theta^{1\times1}_{CO} - k_3\theta^{hex}_{O_{sub}}\theta^{1\times1}_{CO} - k_5\theta^{1\times1}_{CO}\theta^{hex}_{*} + k_{-5}\theta^{hex}_{CO}\theta^{1x1}_{*} + D^{1\times1}_{CO}\frac{\partial^2\theta^{1\times1}_{CO}}{\partial x^2} \quad (4)$$

$$\frac{d\theta^{hex}_{CO}}{dt} = k_2 p_{CO} s^{hex}_{CO}(\theta^{hex} - \theta^{hex}_{CO}) - k_{-2}\theta^{hex}_{CO} - k_4\theta^{hex}_{O_{sub}}\theta^{hex}_{CO} + k_5\theta^{1\times1}_{CO}\theta^{hex}_{*} - k_{-5}\theta^{hex}_{CO}\theta^{1\times1}_{*} + D^{hex}_{CO}\frac{\partial^2\theta^{hex}_{CO}}{\partial x^2} \quad (5)$$

$$\frac{\partial\theta^{hex}_{O_{sub}}}{\partial t} = -k_3\theta^{hex}_{O_{sub}}\theta^{1\times1}_{CO} - k_4\theta^{hex}_{O_{sub}}\theta^{hex}_{CO} \quad (6)$$

$$\frac{\partial\theta^{1\times1}}{\partial t} = k_6\theta^{1\times1}_{CO}(1 - \theta^{1\times1}) - k_7\theta^{hex}_{O_{sub}}\theta^{1\times1} \quad (7)$$

These equations describe the changes in the coverage of CO chemisorbed on the 1 × 1 surface, $\theta^{1\times1}_{CO}$, the coverage of CO on the hex surface, θ^{hex}_{CO}, the coverage of subsurface oxygen under the hex surface, $\theta^{hex}_{O_{sub}}$, and the fraction of the surface in the 1 × 1 phase, $\theta^{1\times1}$. Eqs. (4) and (5) allow CO from the gas phase to adsorb on either the 1 × 1 or hex surfaces (above subsurface oxygen). Conventional terms are used for CO adsorption and desorption on both phases. The kinetics of CO adsorption on the hex phase are assumed to be identical regardless of the presence of subsurface oxygen. Subsurface oxygen also does not block surface sites for CO adsorption. In other words, the hex surface over subsurface oxygen is kinetically identical to the clean hex surface. We propose this as a starting point due to the lack of experimentally determined sticking coefficients and rate constants for the subsurface oxygen hex surface. This assumption also simplifies the model while still capturing the essential mechanistic steps in the process.

Eqs. (4) and (5) also include two different reaction terms. One term, $k_3\theta^{hex}_{O_{sub}}\theta^{1\times1}_{CO}$, allows for reaction between CO on the 1 × 1 surface and the adjacent subsurface oxygen. A second term, $k_4\theta^{hex}_{O_{sub}}\theta^{hex}_{CO}$, allows reaction between subsurface oxygen and CO adsorbed on the hex surface. In other words, subsurface oxygen can react with the CO adsorbed on the surface directly above it. The final terms in the first two equations allow for migration and diffusion of CO. The terms $k_5\theta^{1\times1}_{CO}\theta^{hex}_{*}$ and $k_{-5}\theta^{hex}_{CO}\theta^{1\times1}_{*}$ allow the migration of $CO^{1\times1}$ to hex sites and CO^{hex} to 1 × 1 sites, respectively. Surface diffusion is modeled by Fick's second law.

Eq. (6) is the balance equation for subsurface oxygen and includes two terms, accounting for the two possible reactions with CO. Since there is no chemisorbed oxygen in this model, no formation term is included. The final equation accounts for the surface phase transition. Experiments have shown that subsurface oxygen stabilizes the hex phase, but the removal of subsurface oxygen by CO and subsequent adsorption of CO will cause the lifting of the reconstruction [23]. As in the formation model, the phase transition is modeled by two terms. The first shows that growth of the 1 × 1 phase is proportional to CO coverage, and the second shows that growth of the hex phase is proportional to the subsurface oxygen coverage. This simple model does not fully capture the physics of the surface phase reconstruction. For instance, the effect on the surface phase of CO adsorbed on top of the subsurface oxygen hex phase is not addressed, nor is the full adsorbate-induced reconstruction model included. The factors will need to be addressed in any full CO oxidation model that includes subsurface oxygen.

The problem is solved in one dimension with no-flux boundary conditions on all variables and the initial conditions shown in Fig. 7. Initially, a subsurface oxygen island 500 μm in diameter is surrounded by a clean 1 × 1 surface. This initial condition is a simplification because the clean surface should reconstruct to the hex phase, but

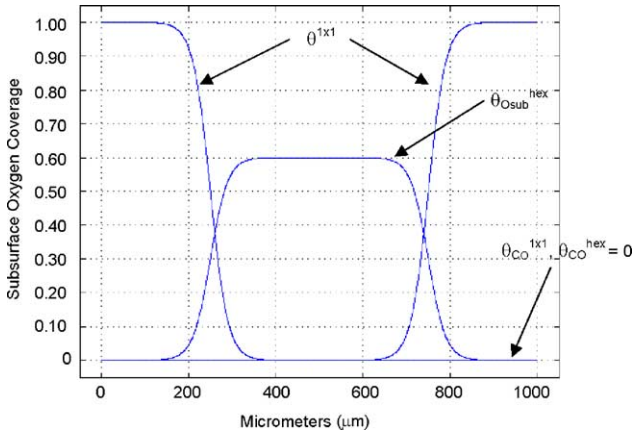

Fig. 7. Initial conditions for simulations of the removal of subsurface oxygen by CO.

Table 2
List of values used in PDE model for reactive removal of subsurface oxygen

Parameter	Value		Reference
	Pre-exponential	Activation energy (kJ/mol)	
k_1	2.92×10^5 s^{-1} Torr^{-1}	0	[27]
k_{-1}	1×10^{15} s^{-1}	154	[27]
k_2	2.92×10^5 s^{-1} Torr^{-1}	0	[27]
k_{-2}	1×10^{15} s^{-1}	154	[27]
k_3	3×10^6 s^{-1}	62	[23,28]
k_4	3×10^6 s^{-1}	100	[28]
k_5	1×10^4 s^{-1}	49	[27]
k_{-5}	43 s^{-1}	0	[27]
k_6	0.01 s^{-1}	0	–
k_7	0.01 s^{-1}	0	–
$D_{CO}^{1\times1}$	0.075 cm^2 s^{-1}	48	[28]
D_{CO}^{hex}	0.075 cm^2 s^{-1}	48	[28]

Parameter	Value	Reference
$S_{CO}^{1\times1}$	0.91	[3]
S_{CO}^{hex}	0.78	[3]

adsorption of CO will quickly lift this reconstruction. At time = 0, the partial pressure of CO, p_{CO}, is increased. Table 2 lists the values of all parameters used for this simulation. The general result of the simulation is the removal of the subsurface oxygen island predominantly from the edges inward, similar to the behavior that is observed experimentally.

Simulations were performed for several values of p_{CO} between 10^{-4} mbar and 10^{-8} Torr. Results are in qualitative agreement with experiments, as can be seen in Fig. 8. The subsurface island is removed from the edges with an average front velocity of 1.8 μm/s. This velocity is highly dependent on the partial pressure of CO. Fig. 9 shows the same simulation but with a higher CO pressure. In this case, the removal from the edges occurs more quickly, around 3.2 μm/s. Furthermore, the reaction of subsurface oxygen occurs as much in the interior of the subsurface oxygen island as from the edges.

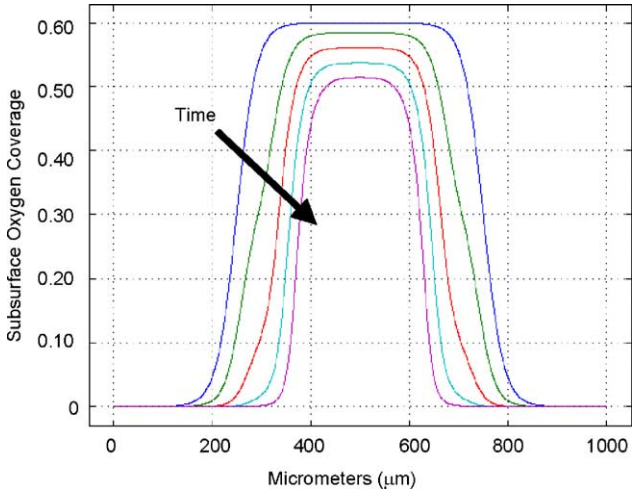

Fig. 8. Simulation of the removal of subsurface oxygen at 500 K and $p_{CO} = 1 \times 10^{-7}$ Torr shown from 0 to 80 s. Profiles are at 20 s intervals.

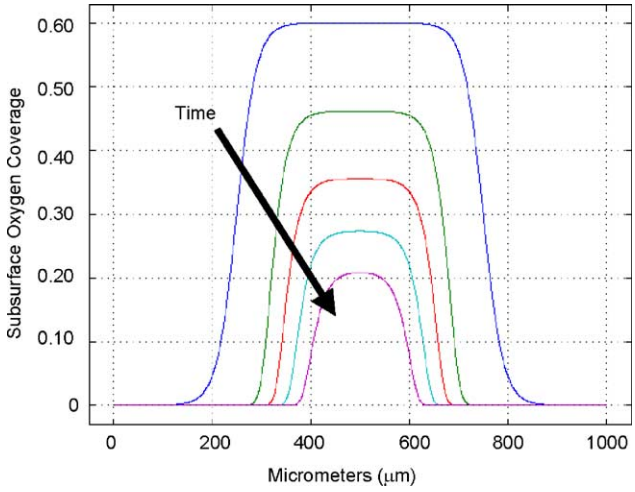

Fig. 9. Simulation of the removal of subsurface oxygen at 500 K and $p_{CO} = 1 \times 10^{-4}$ Torr shown from 0 to 80 s. Profiles are at 20 s intervals.

The results of the two models just presented validate qualitatively the proposed mechanism for the formation and reaction of subsurface oxygen. The simulations show that several experimental observations of subsurface oxygen can be explained by fundamental surface processes alone. A better understanding of the effect of subsurface oxygen on the surface phase transition is necessary in order to make these results quantitative.

4. Conclusion

The experiments discussed here have shown that subsurface oxygen has a profound effect on the reaction dynamics of CO oxidation on Pt(1 0 0), contributing to spatiotemporal pattern formation and changes in reaction dynamics. This paper has emphasized that subsurface oxygen is not identical to chemically inactive surface oxide or bulk oxides. Instead, subsurface oxygen actively participates in chemical reactions, as shown for the first time at intermediate pressures by EMSI.

Microkinetic models have provided additional insight into the formation of subsurface oxygen. Simulation results show that fundamental surface processes can account for the formation and reactive removal of subsurface oxygen. A combination of the two models discussed in this paper should lead to a comprehensive model for subsurface oxygen formation and removal under reaction conditions at low pressures. Such a model is valuable because it would provide information about global variables such as reaction rate as well as information about pattern formation. Future experimental and modeling work will focus on further investigation of the relationship between the surface phase transition and the formation of subsurface oxygen.

References

[1] T. Lele, J. Lauterbach, Chaos 12 (2002) 164.
[2] R. Imbihl, M.P. Cox, G. Ertl, J. Chem. Phys. 84 (1986) 3519.
[3] M.M. Slin'ko, N.I. Jaegar, Oscillating Heterogeneous Catalytic Systems, Elsevier, Amsterdam, 1994.
[4] M.A. Barteau, E.I. Ko, R.J. Madix, Surf. Sci. 104 (1981) 161.
[5] P.R. Norton, J.A. Da Vies, D.K. Creber, C.W. Sitter, T.E. Jackman, Surf. Sci. 108 (1981) 205.
[6] M.A. Barteau, E.I. Ko, R.J. Madix, Surf. Sci. 102 (1981) 99.
[7] J.E. Turner, B.C. Sales, M.B. Maple, Surf. Sci. 103 (1980) 54.
[8] T. Matsushima, D.B. Almy, J.M. White, Surf. Sci. 67 (1977) 89.
[9] C.E. Smith, JB. Biberian, G.A. Somorjai, J. Catal. 57 (1979) 426.
[10] S. Ladas, R. Imbihl, G. Ertl, Surf. Sci. 219 (1989) 88.
[11] M. Soick, O. Buyevskaya, M. Hohenberger, D. Wolf, Catal. Today 32 (1996) 163.
[12] M. Fathi, F. Monnet, Y. Schuurman, A. Holmen, C. Mirodatos, J. Catal. 190 (2000) 439.
[13] E.P.J. Mallens, L.H.B.J. Hoebink, G.B. Marin, Catal. Lett. 33 (1995) 291.
[14] J. Dicke, H.H. Rotermund, J. Lauterbach, Surf. Sci. 454–456 (2000) 352.
[15] H.H. Rotermund, W. Engel, S. Jakubith, A. von Oertzen, G. Ertl, Ultramicroscopy 36 (1991) 164.
[16] H.H. Rotermund, G. Haas, R.U. Franz, R.M. Tromp, G. Ertl, Appl. Phys. A: Mater. Sci. Process. 61 (1995) 569.
[17] G. Haas, R.U. Franz, H.H. Rotermund, R.M. Tromp, G. Ertl, Surf. Sci. 352 (1996) 1003.
[18] H.H. Rotermund, Surf. Sci. Rep. 29 (1997) 367.
[19] G. Haas, T.D. Pletcher, G. Bonilla, TA. Jachimowski, H.H. Rotermund, J. Lauterbach, J. Vac. Sci. Technol. A: Vac. Surf. Films 16 (1998) 1117.
[20] H.H. Rotermund, W. Engel, S. Jakubith, A. von Oertzen, G. Ertl, Ultramicroscopy 36 (1991) 164.
[21] H.H. Rotermund, J. Lauterbach, G. Haas, Appl. Phys. A 57 (1993) 507.
[22] P.R. Norton, K. Griffiths, P.E. Bindner, Surf. Sci. 138 (1984) 125.
[23] J. Lauterbach, K. Asakura, H.H. Rotermund, Surf. Sci. 313 (1994) 52.
[24] T. Lele, T.D. Pletcher, J. Lauterbach, AIChE J. 47 (2001) 1418.
[25] K. Krischer, M. Eiswirth, G. Ertl, J. Chem. Phys. 96 (1992) 9161.
[26] T. Lele, J. Lauterbach, D. Ramkrishna, AIChE J. 49 (2003) 2158.
[27] M. Gruyters, T. Ali, D.A. King, J. Phys. Chem. 100 (1996) 14417.
[28] A. von Oerzten, A. Mikhailov, H.H. Rotermund, G. Ertl, Surf. Sci. 350 (1996) 259.
[29] A. von Oerzten, A. Mikhailov, H.H. Rotermund, G. Ertl, J. Phys. Chem. B 102 (1998) 4966.
[30] A. von Oerzten, H.H. Rotermund, A. Mikhailov, G. Ertl, J. Phys. Chem. B 104 (2000) 3155.